Effects of B_2O_3 and BaO on the Crystallization Behavior of CaO-Al_2O_3-Based Mold Flux for Casting High-Al Steels

DAN XIAO, WANLIN WANG, and BOXUN LU

The non-reactive lime–alumina-based mold flux has been proposed to overcome the aluminum introduced slag/steel interaction problems during the casting of high aluminum bearing steels. In this article, a new mold flux with CaO/Al_2O_3 (C/A) ratio of 2 was designed, and the effects of BaO substituting for CaO to replace B_2O_3 on the mold flux crystallization behaviors have been investigated through the using of single hot thermocouple technology and double hot thermocouple technology (DHTT). The results suggested that BaO shows the stronger tendency to inhibit crystallization of mold flux comparing with B_2O_3; however, the synergic effect of the combination of BaO and B_2O_3 tends to improve the mold flux crystallization in this non-reactive mold flux system. The analysis of the crystallized phases for different samples and the crystallization behaviors under simulated thermal gradient through DHTT were also conducted to support the reliability of above conclusions.

DOI: 10.1007/s11663-014-0286-6

I. INTRODUCTION

MOLD flux has been widely used in continuous casting,[1] to play important roles such as lubricating the strand, absorbing inclusions from liquid steel, preventing the steel from oxidation, and moderating the heat transfer between the steel and mold.[2] In order to meet the production needs of advanced auto body steel, the research regarding to Advanced High Strength Steels (AHSS) has been conducted intensively, especially for the transformation-induced plasticity (TRIP) steels.[3] However, a large quantity of aluminum has been added in TRIP steel, and the high Al in the molten steel has the tendency to react with SiO_2 in the mold slag during the process of continuous casting; therefore, the content of SiO_2 in the mold slag decreases markedly and Al_2O_3 increases obviously. Consequently, the properties of the resulting mold flux vary dramatically, and would tend to cause the lubrication and heat transfer problems, which in turn introduce poor surface quality of the cast slabs. Previous studies regarding to the optimization of the ratio of Al_2O_3/SiO_2[4,5] or CaO/SiO_2[6,7] and the amount of fluidizers[8,9] for the traditional lime–silica-based mold flux to solve these problems have been conducted. However, the variance of crystallization and heat flux behaviors of mold flux that introduced by slag/steel reaction make it difficult to optimize above mold fluxes system.

Therefore, the non-reactive lime–alumina-based mold flux has been proposed, where SiO_2 has been partially replaced by Al_2O_3 to inhibit the reaction between Al and SiO_2 (slag/steel interaction) in the casting of high-Al TRIP steels. Cho *et al.*[10] investigated a series of lime–alumina-based mold fluxes with CaO/Al_2O_3 (C/A) ratio of 1 and 3.3 in casting experiments; and the trial results of the mold flux with C/A of 1 indicate that the fluctuation of final spent mold flux has been inhibited comparing with lime–silicate-based system, but the final spent mold fluxes show strong crystallization property that leads to the deterioration of the mold lubrication. Meanwhile, the trail results of C/A 3.3 suggest that even though the problem of lubrication became better, however, the fluctuation of heat flux and slag/steel reaction was getting stronger than those of C/A 1, also the spent mold fluxes show strong crystallization tendency. Therefore, the study of the lime–alumina-based mold flux with C/A of 2 is worthy to be studied, as it has the potential to improve the lubrication property in the casting of high-Al TRIP steel compared with mold fluxes with C/A of 1. Meanwhile, it can reduce slag/steel reaction comparing with mold fluxes with C/A of 3.3.

As the problem of strong crystallization of previous developed mold flux system, fluxing agents like B_2O_3 and BaO have been widely used to lower the melting and solidification temperature[11] and restrain mold flux crystallization.[12] However, high B_2O_3 content of mold flux will introduce additional slag interaction with [Al] containing in the molten steel. Moreover, research suggested that BaO substituting for CaO plays a similar role as that of B_2O_3,[13,14] which can decrease melting temperature and inhibit crystallization. Therefore, it is possible to use the substitution of BaO for CaO to replace B_2O_3 to optimize the non-reactive lime–alumina-based mold flux system.

Consequently, it is essential to first look at the crystallization behavior of the lime–alumina-based slag system when the C/A is around 2, as this one has the potential to avoid the slag/steel interaction and improve the mold flux lubrication capability. Based on this assumption, the effect of BaO substituting for CaO to

DAN XIAO and BOXUN LU, Graduate Students, and WANLIN WANG, Professor, are with the School of Metallurgy and Environment, Central South University, Changsha 10083, P.R. China. Contact e-mail: wanlin.wang@gmail.com

Manuscript submitted December 7, 2014.
Article published online January 10, 2015.

Table I. The Major Chemical Compositions of Mold Fluxes with Different B_2O_3 and BaO Contents (in Mass Pct)

Sample	CaO	SiO_2	Al_2O_3	Na_2O	Li_2O B_2O_3 BaO
1	37.33	9	18.67	10	6 10 0
2	37.00	9	20.00	10	6 6 3
3	34.33	9	20.67	10	6 4 7
4	34.00	9	22.00	10	6 0 10

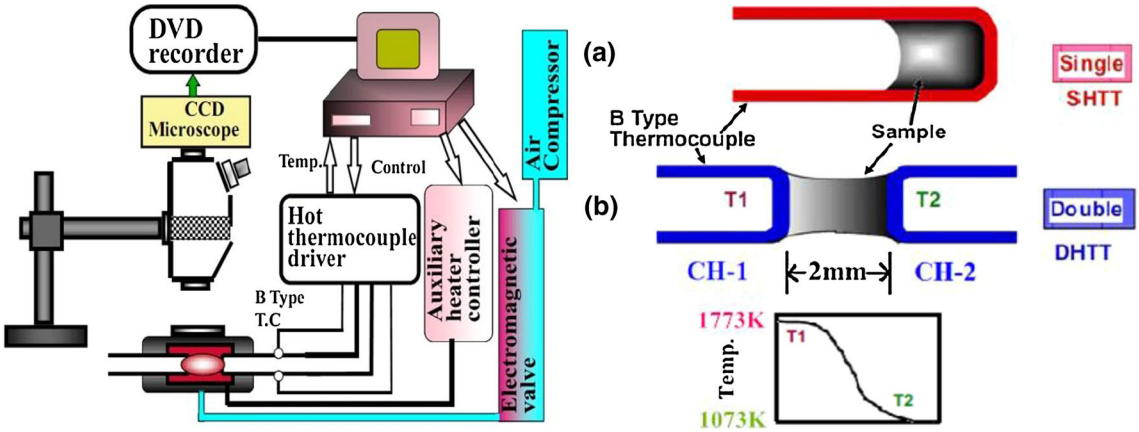

Fig. 1—The schematic of (*a*) single and (*b*) double hot thermocouples.

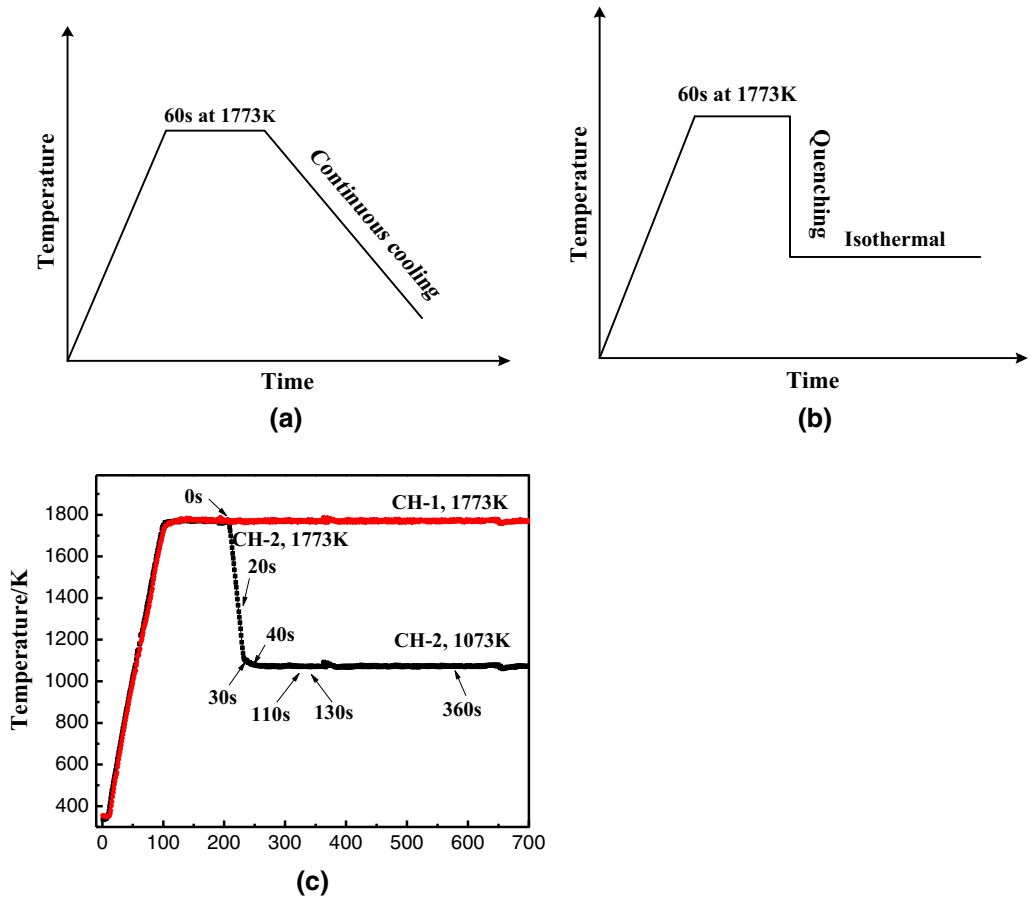

Fig. 2—Thermal profiles of (*a*) CCT, (*b*) TTT, and (*c*) DHTT experiments.

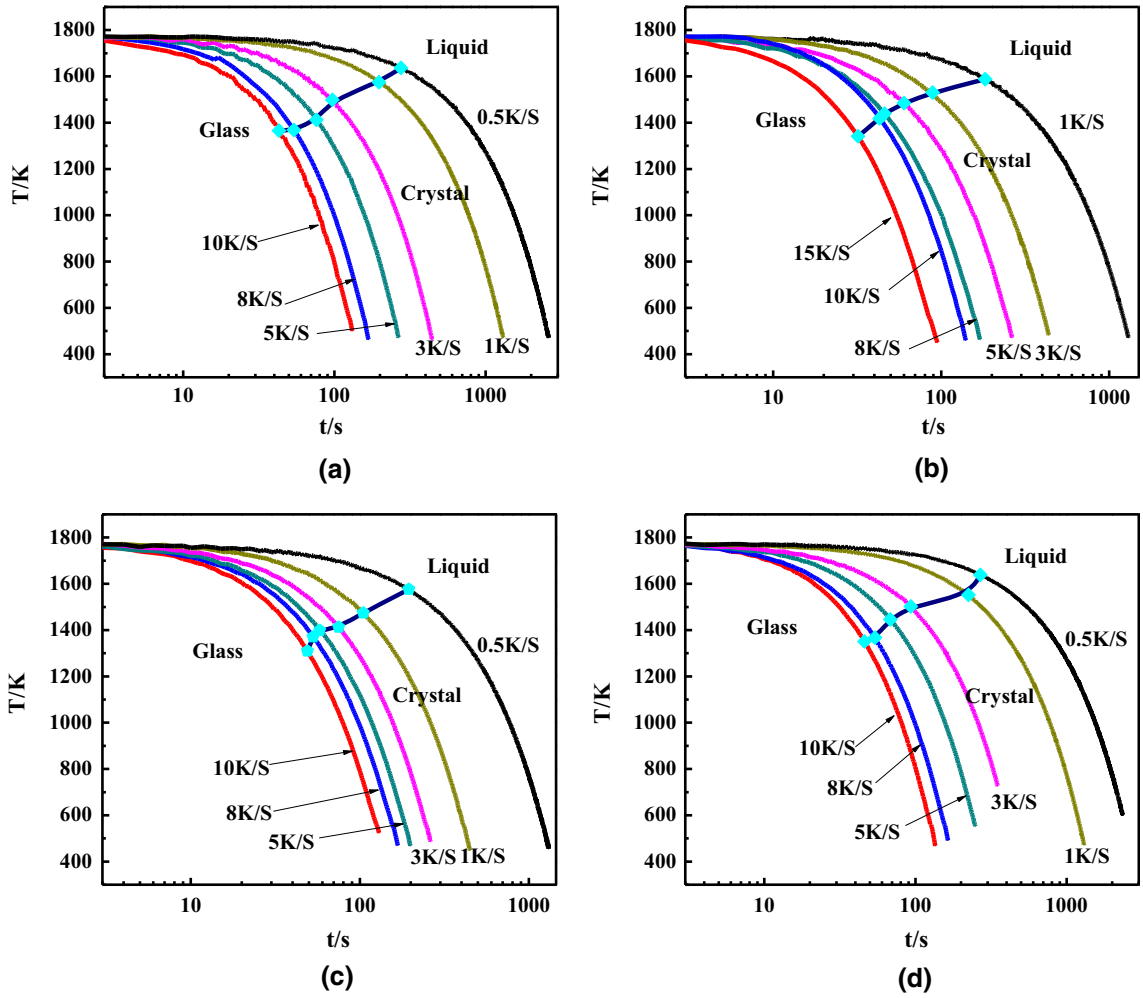

Fig. 3—CCT diagrams of slag sample with different B_2O_3 and BaO contents: (*a*) sample 1: B_2O_3 = 10 mass pct, BaO = 0 mass pct; (*b*) sample 2: B_2O_3 = 6 mass pct, BaO = 3 mass pct; (*c*) sample 3: B_2O_3 = 4 mass pct, BaO = 7 mass pct; (*d*) sample 4: B_2O_3 = 0 mass pct, BaO = 10 mass pct.

Table II. The Initial Crystallization Temperature of Different Sample at a Cooling Rate of 8 K/s

B_2O_3 (mass pct)	BaO (mass pct)	Critical Cooling Rate (K/S)	Initial Crystallization Temperature (K)
10	0	10	1368.07
6	3	15	1439.40
4	7	10	1370.78
0	10	10	1348.05

replace B_2O_3 on the crystallization behavior needs to be conducted to avoid the potential interaction between high content of B_2O_3 in the slag and the [Al] in the molten steel. The results of this study would provide guideline for the design of lime–alumina-based mold flux for casting of high-aluminum TRIP steels.

II. EXPERIMENTAL APPARATUS AND PROCESS

A. *Materials*

The designed samples (Sample 2, 3 and 4) for the study were based on the major composition of sample 1 in Table I, and they were obtained according to the principle that reduce B_2O_3 content and substitute BaO for CaO simultaneously, meanwhile keep (CaO + BaO)/Al_2O_3 ratio and other oxides content constant. The major chemical compositions of the samples are shown in Table I; they were prepared by pure chemical regents $CaCO_3$, SiO_2, Al_2O_3, Na_2CO_3, Li_2CO_3, B_2O_3, and $BaCO_3$. The pure chemicals were melted in a graphite crucible, which was placed into an induction furnace, at 1773 K (1500 °C) for 300 seconds to homogenize its chemical composition and eliminate bubbles. Then, the mold flux was poured into water for quenching to obtain fully glassy phase flux. Next, the glassy sample was dried, crushed, and ground into sample powders for the

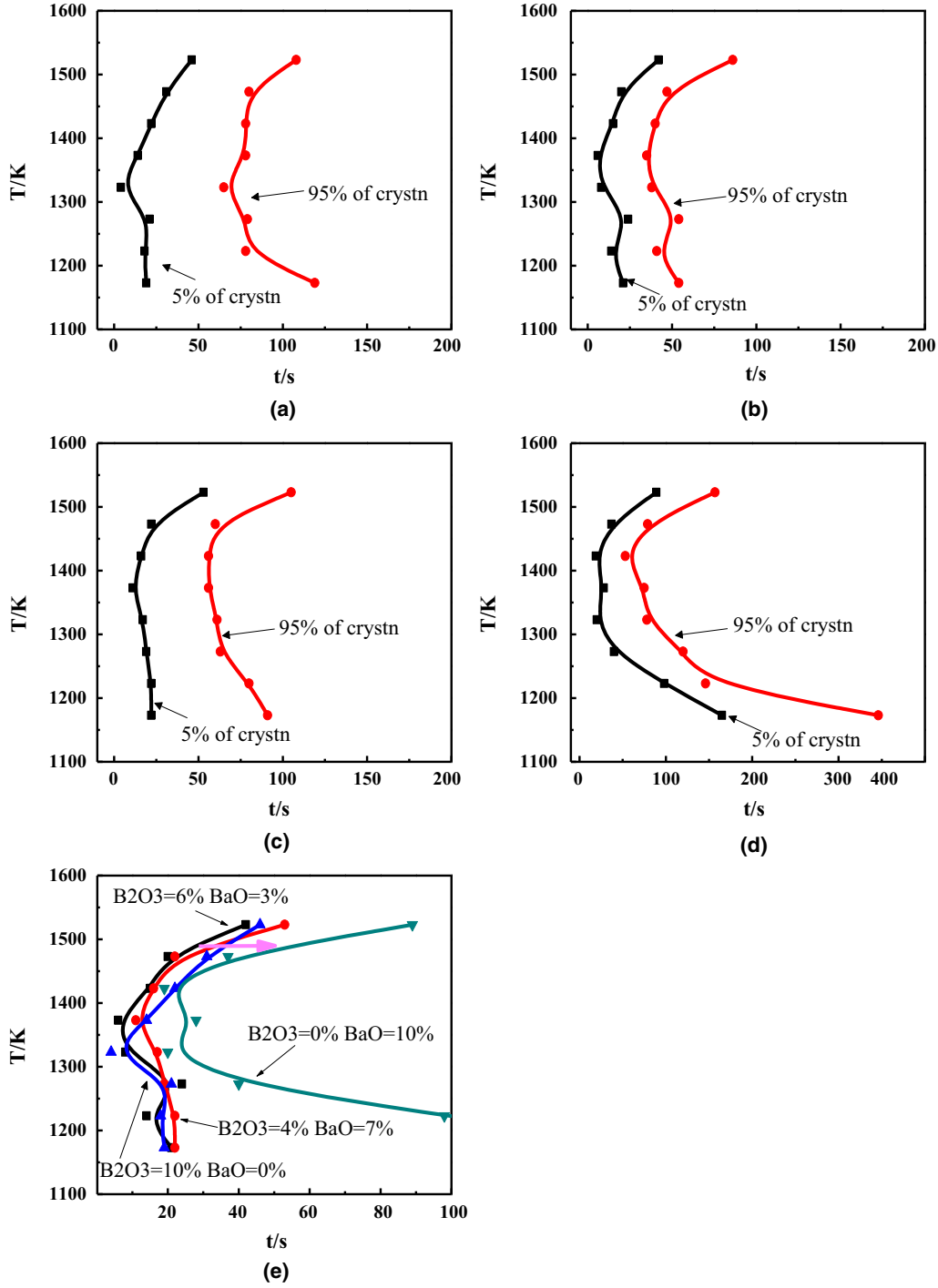

Fig. 4—TTT diagrams of slag sample with different B_2O_3 and BaO contents: (*a*) sample 1: B_2O_3 = 10 mass pct, BaO = 0 mass pct; (*b*) sample 2: B_2O_3 = 6 mass pct, BaO = 3 mass pct; (*c*) sample 3: B_2O_3 = 4 mass pct, BaO = 7 mass pct; (*d*) sample 4: B_2O_3 = 0 mass pct, BaO = 10 mass pct, and (*e*) four TTT curves combined.

following single hot thermocouple technology (SHTT) and double hot thermocouple technology (DHTT) tests.

B. *Apparatus and Method*

The continuous cooling transformation (CCT) and time temperature transformation (TTT) experiments were conducted by using SHTT, and the crystallization experiments under simulated thermal gradient were conducted by using DHTT. Figure 1 shows the schematic figure of SHTT/DHTT, and the details have been given in our previous studies.[15]

In this study, the beginning and end of crystallization are defined by the 5 pct of crystallization and 95 pct of crystallization, respectively.[16] During the cooling process, the temperature at which 5 pct of crystallization

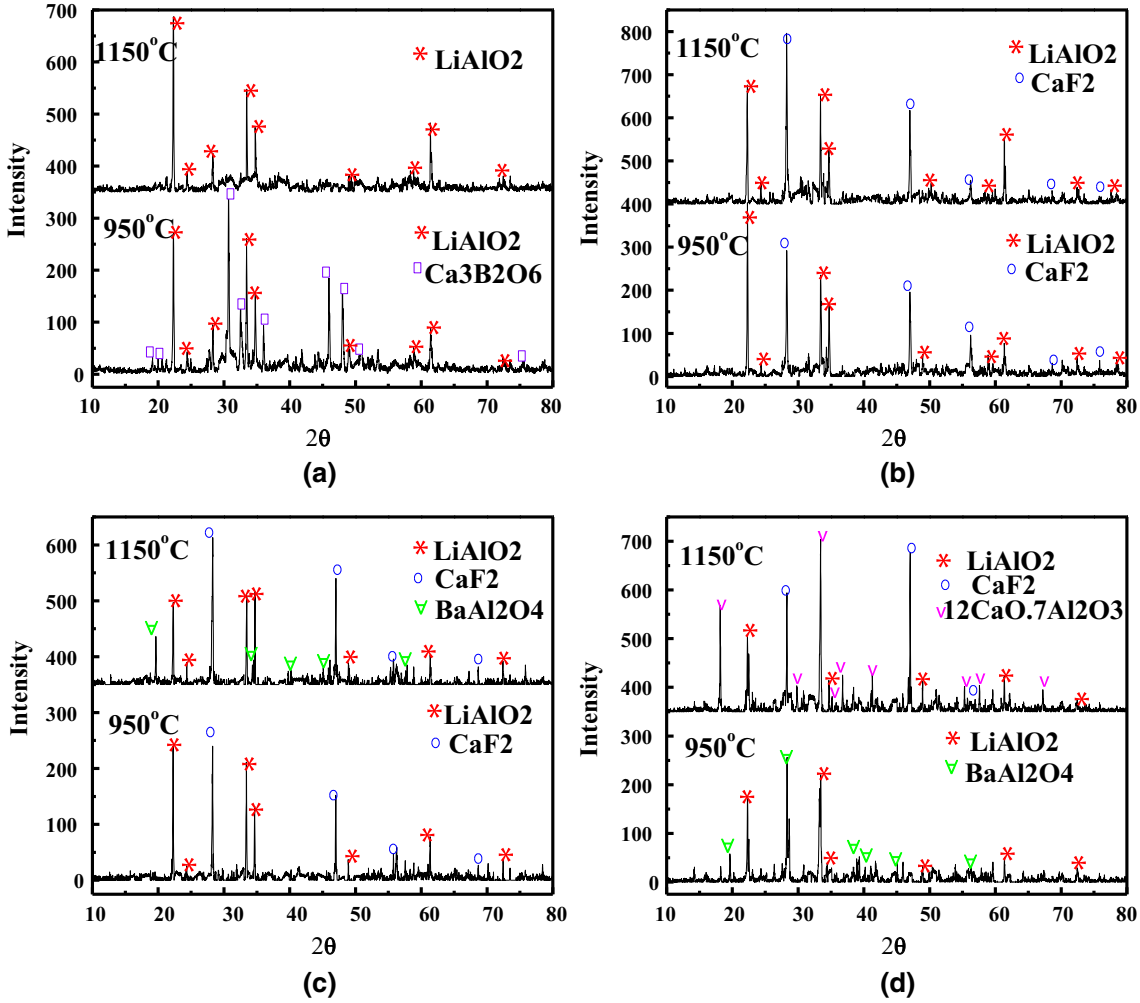

Fig. 5—X-ray diffraction patterns of slag sample with different B_2O_3 and BaO contents: (*a*) sample 1: B_2O_3 = 10 mass pct, BaO = 0 mass pct; (*b*) sample 2: B_2O_3 = 6 mass pct, BaO = 3 mass pct; (*c*) sample 3: B_2O_3 = 4 mass pct, BaO = 7 mass pct; (*d*) sample 4: B_2O_3 = 0 mass pct, BaO = 10 mass pct.

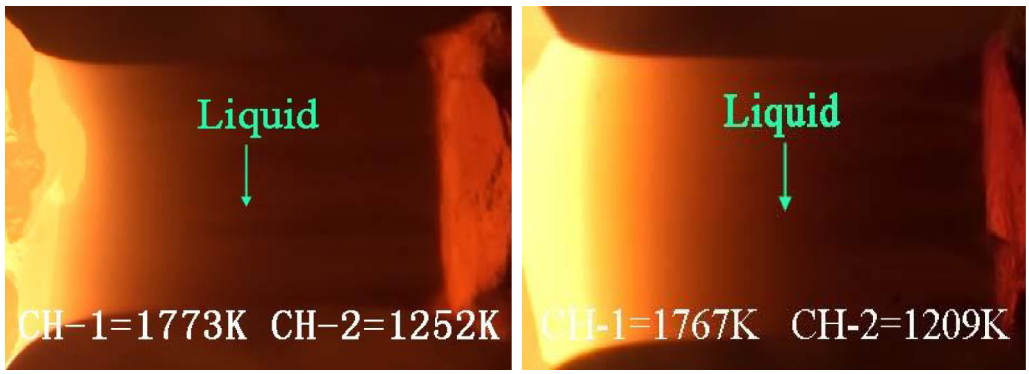

(a) 20s **(b)** 20s

Fig. 6—The DHTT diagrams when the holding time is 20 s: (*a*) sample 1: B_2O_3 = 10 mass pct, BaO = 0 mass pct; (*b*) sample 4: B_2O_3 = 0 mass pct, BaO = 10 mass pct.

was defined as the initial crystallization temperature. The schematic illustration of the SHTT experimental apparatus is shown in Figure 1(a), the slag powders sample was mounted on one thermocouple, which could be heated directly, while computer system is used to record the temperature simultaneously. Figures 2(a) and (b) show the thermal profiles for CCT and TTT experiments. For CCT experiments, the slag powders

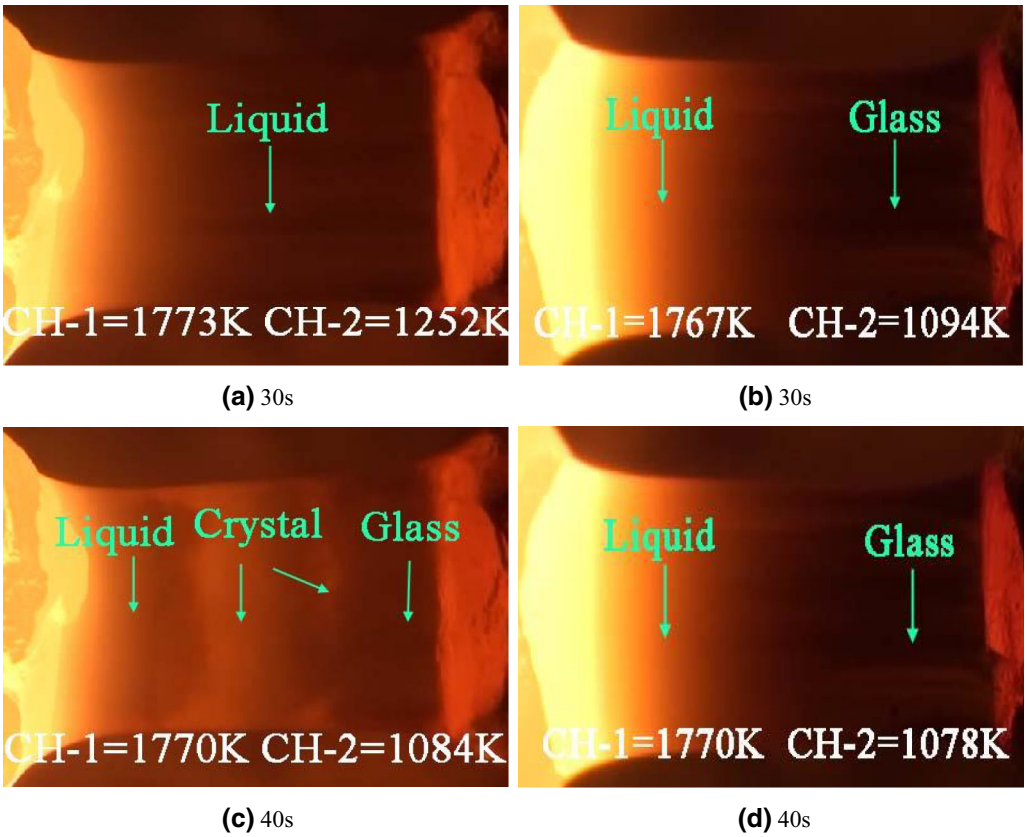

(a) 30s **(b)** 30s

(c) 40s **(d)** 40s

Fig. 7—The DHTT diagrams when the holding time is 30 and 40 seconds: (*a*, *c*) sample 1: B_2O_3 = 10 mass pct, BaO = 0 mass pct; (*b*, *d*) sample 4: B_2O_3 = 0 mass pct, BaO = 10 mass pct.

sample was mounted on a B-type thermocouple, and it was heated from room temperature to 1773 K (1500 °C) at a rate of 900 K/min and held for 60 seconds to eliminate bubbles in molten slag and homogenize its chemical composition. Then, the molten slag sample was cooled at different cooling rates. For TTT experiment, the slag powder sample was also heated from room temperature to 1773 K (1500 °C) at a rate of 900 K/min, and then it was held for about 60 seconds. Then, the molten slag was then cooled at 1800 K/min to different temperatures for isothermal crystallization. The CCT and TTT diagrams were conducted by recording the relationship between time, temperature, and transformation.

The X-ray diffraction (XRD) was employed to identify the phase composition of crystals precipitated in the mold flux. The XRD data were collected in a range of 2θ = 10 to 80 deg with a step size of 10 deg/min using Cu Kα radiation (1.54184 Å).

The illustration of DHTT is shown in Figure 1(b), and the slag powders sample was installed between two B-type thermocouples, and through control the temperature of each thermocouple, respectively, to achieve the desired temperature gradient between the two thermocouples. The hot thermocouple (CH-1) and cold thermocouple (CH-2) were set as 1773 K (1500 °C) and 1073 K (800 °C), respectively to simulate the shell surface temperature and cold mold flux interface temperature.[17] Figure 2(c) shows the thermal profiles for DHTT experiments, where the slag powders were installed on one of B-type thermocouple, and heated from room temperature to 1773 K (1500 °C) at a rate of 900 K/min and held for about 60 seconds to eliminate bubbles in molten slag and homogenize its chemical composition; next, the slag sample was elongated to 2 mm through the other thermocouples. Then the cold thermocouple (CH-2) was cooled and maintained at 1073 K (800 °C), to observe the crystallization of mold flux.

III. RESULTS AND DISCUSSION

A. *Effect of BaO Substituting for CaO to Replace B_2O_3 on the Crystallization Behavior of Mold Flux*

Figure 3 shows the CCT diagram for four slag samples, and the results of CCT curves show that the crystallization temperature reduces with the increase of continuous cooling rate. The phenomenon may be due to fact that viscosity of mold flux and degree of undercooling can determine the nucleation and growth rate of crystals. With the increase of cooling rate, the viscosity of the mold flux increases. It requires larger driving force to initiate mold flux crystallization, which means the crystallization temperature is getting lower.

The critical cooling rate is defined as the cooling rate at which there is no crystallization occurs, it is an

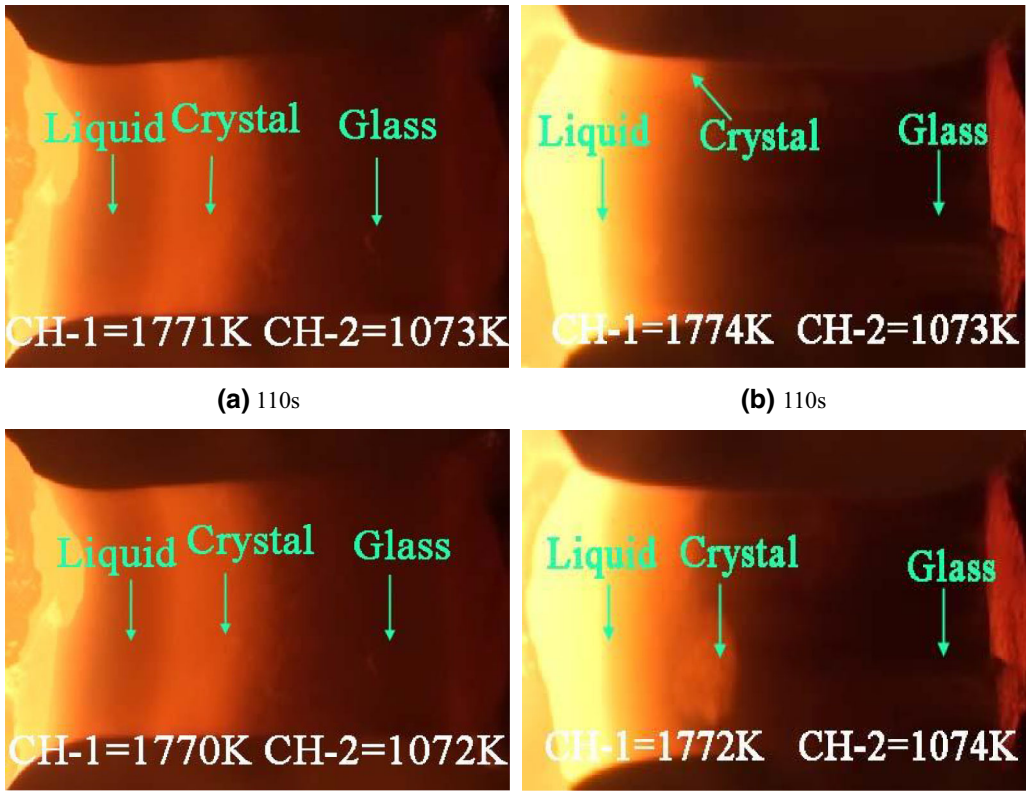

(a) 110s **(b)** 110s

(c)130s **(d)** 130s

Fig. 8—The DHTT diagrams when the holding time is 110 and 130 s: (*a*, *c*) sample 1: B_2O_3 = 10 mass pct, BaO = 0 mass pct; (*b*, *d*) sample 4: B_2O_3 = 0 mass pct, BaO = 10 mass pct.

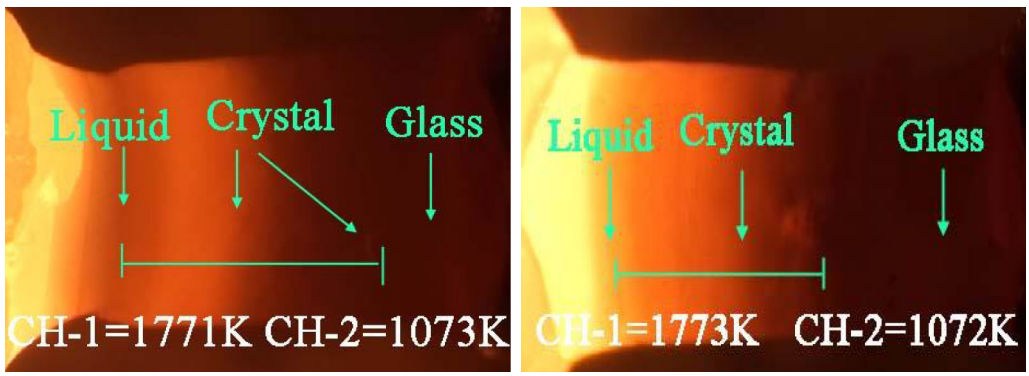

(a) 360s **(b)** 360s

Fig. 9—The DHTT diagrams when the holding time is 360 s: (*a*) sample 1: B_2O_3 = 10 mass pct, BaO = 0 mass pct; (*b*) sample 4: B_2O_3 = 0 mass pct, BaO = 10 mass pct.

important index to characterize the crystallization properties of mold flux. The critical cooling values for Sample 1, Sample 2, Sample 3, and Sample 4 are 10, 15, 10, and 10 K/S, respectively, as shown in Figure 3. It could be observed that the critical cooling rate increases when 10 pct B_2O_3 was replaced by 6 pct B_2O_3 and 3 pct of BaO, which indicates that using 3 pct BaO substituting for CaO to replace 4 pct B_2O_3 can promote crystallization (Sample 2). While B_2O_3 pct decreases from 10 pct to 4 pct and 0 pct, and BaO pct increases from 0 pct to 7 pct and 10 pct (Sample 1, 3, and 4), the critical cooling rate remains unchanged.

The initial crystallization temperature of different mold fluxes at a cooling rate of 8 K/s is shown in Table II. The initial crystallization is changed from 1368.07 K to 1439.40 K, 1370.78 K, and 1348.05 K (1095.07 °C to 1166.4 °C, 1097.78 °C, and 1075 °C) with the decrease of B_2O_3 content from 10 to 6, 4, and 0 pct, and the increase of BaO content from 0 to 3, 7, and 10 pct. The initial crystallization temperature of

Sample 4 is a little bit lower than that of Sample 1. Thus, it indicates that Sample 4 has a stronger ability to inhibit crystallization than that of Sample 1.

The above results also suggest that with the substitution of BaO for CaO to replace B_2O_3, the crystallization capability of mold flux is getting improved, such that the critical cooling rate and crystallization temperature of Sample 2 are highest among all samples. The interesting phenomenon is that with the further addition of BaO to substitute CaO to replace B_2O_3, such as Sample 3, its crystallization temperature and critical cooling rate reduce; however, its crystallization temperature is still higher than Sample 1 and 4, even though their critical cooling temperatures are keeping same, which suggest that the synergic effect of the combination of BaO and B_2O_3 would tend to improve the crystallization behavior of the slag system. Through the comparison of Sample 1, 3, and 4, it can be found that pure BaO has a weaker crystallization capability than that of B_2O_3, such that Sample 4 shows lowest crystallization temperature.

The TTT diagrams of mold fluxes for above 4 mold fluxes are shown in Figure 4, and all TTT curves are combined together in Figure 4(e). First, it could be observed that BaO would restrain the mold flux crystallization more dramatically, such that it would take longest time to initiate the crystallization than others, especially during the low-temperature zone, where it could be observed that it takes more than 100 seconds to initiate crystallization for Sample 4 when the holding temperature goes down to 1000 K (727 °C). Also the Sample 2 with the mixture of 6 pct B_2O_3 and 3 pct BaO shows strongest crystallization capability, as its incubation time is shortest. Followed by Sample 3 with the mixture of 4 pct B_2O_3 and 7 pct BaO, it shows quite strong crystallization capability in high-temperature zone. However, the variation of the content of BaO and B_2O_3 does not have significant effect on the mold flux crystallization during the low-temperature zone. Those results are consistent with the CCT results as listed in Table II.

The reason for the above interesting phenomena may be explained as follows: in CaO-Al_2O_3-based mold flux system, compared with the traditional CaO-SiO_2-based mold flux, SiO_2 was partially replaced by Al_2O_3, leading to the major network changed from the $[SiO_4]^{4-}$ structure to large and more complex $[AlO_2]^-$ structure, so the degree of polymerization of mold flux increases. BaO is alkaline oxides, the addition of BaO would promote the forming of acid network.[18] Addition of alkali metal ions(Ba^{2+}) can compensate $[AlO_2]^-$ valence to form more complex and stable network structure, like $BaAl_2O_4$. Thus, it makes mold flux more difficult to crystallize with the addition of BaO. The formation of $BaAlO_4$ in Sample 3 and 4 (Figures 5(c) and (d)) is the evidence of this proposal (Section B). B_2O_3 is generally accepted as a network former; $[BO_3]^{3-}$ triangular unit and $[BO_4]^{5-}$ tetrahedral unit are the base structure units of borate network, and those units are difficult to move and contribute to form vitreous bodies. Meanwhile, the borate network could be combined into silicate network, which makes the network structure more complex; therefore, B_2O_3 could restrain the crystallization of mold flux. The formation of $Ca_3B_2O_6$ in Sample 1 in Figure 5(a) is the evidence of this proposal. However, with the partial substitution of BaO for CaO to replace B_2O_3, the solubility of $[O]^{2-}$ increased with the addition of BaO, and it makes network structure disconnected, which is favorable for improving the crystallization ability, such that CaF_2 would form in Samples 2, 3, and 4 as shown in Figures 5(b), (c), and (d). So, the mixture of BaO and B_2O_3 has the stronger crystallization capability. If there are more BaO added into system, $BaAl_2O_4$ phase will form and the effect of BaO to inhibit crystallization will be dominant.

B. *XRD Results of the Mold Flux Crystallization*

The crystal phase of the above samples after experiment was analyzed by XRD, and their results are shown in Figure 5. It could be seen that $LiAlO_2$ crystal is appearing in both high- and low-temperature zones for all samples, which suggest that the $[AlO_2]^-$ structure is the major network structure in the non-reactive mold flux system. In Figure 5(a), the crystal phase of CaB_2O_3 is formed in the low-temperature zone, which is the evidence of the proposal that B_2O_3 tends to inhibit mold flux crystallization. With more addition of BaO to replace B_2O_3, CaF_2 crystals precipitate in both high and low-temperature zone for both Sample 2 and Sample 3 as shown in Figures 5(b) and (c). The reason for the precipitation of CaF_2 may be explained as that B_2O_3 has the effect to inhibit the formation of CaF_2,[19] and CaF_2 is easy to precipitate in high temperature as suggested in previous studies.[3] Therefore, the precipitation of CaF_2 in Sample 2 and 3 with the reduction of B_2O_3 explains that Sample 2 and Sample 3 show high crystallization temperature in high-temperature zone as suggested in above TTT and CCT results. With the further addition of BaO, $BaAl_2O_4$ is precipitated in the high-temperature zone or in low-temperature zone for Sample 3 and 4 as shown in Figures 5(c) and (d), which is also the evidence for the proposal that BaO tends to inhibit mold flux crystallization. While $12CaO{\cdot}7Al_2O_3$ is precipitated in high-temperature zone and $BaAl_2O_4$ is formed in low-temperature zone for Sample 4 as shown in Figure 5(d), when B_2O_3 content is fully replaced by 10 pct BaO; as $12CaO{\cdot}7Al_2O_3$ and $BaAl_2O_4$ are major phases appearing in the high-temperature and low-temperature zone for Sample 4, respectively, which is very difficult to form that may explain why Sample 4 showing strongest capability to inhibit crystallization.

C. *Crystallization Behavior of Mold Flux Under Simulated Thermal Gradient*

From the results of CCT and TTT, it could be concluded that the pure BaO has the stronger ability to inhibit crystallization than that of B2O3. In order to further elucidate above phenomenon, the DHTT was employed to conduct the crystallization behavior of Sample 1 and Sample 4 under simulated thermal gradient. The DHTT images of the two mold fluxes that have been exposed to the temperature gradient of 1773 K and 1073 K (1500 °C and 800 °C) for same

times were compared, as shown in Figures 6 through 9. When the holding time was 20 seconds, it was observed that there is no crystal precipitated in Sample 1 and Sample 4. Figure 7 shows the DHTT images when the holding times are 30 and 40 seconds. Figure 7(a) shows that a few crystals were appearing in middle area for Sample 1, and from Figures 7(a) through (c), the crystals mainly grow toward the high-temperature region for Sample 1. However, there is still no crystals appearing in Sample 4, and large glassy phase was formed at the cold end. The results indicate that the crystallization property of Sample 4 is weaker than Sample 1, which is consistent with the TTT results above.

When the holding time became 110 seconds as shown in Figure 8, it can be observed that mold fluxes have shown three layers, *i.e.*, liquid, crystal, and glassy layers for Sample 1. For Sample 4, the crystals were precipitated in higher temperature region close to thermocouple (CH-1). When the holding time becomes 130 seconds, for Sample 4, the crystals are growing toward the low-temperature region, and the low-temperature zone still keeps glassy phase, which matches well with the TTT curves in Figure 4(e) where the crystallization of Sample 4 is greatly restrained in the low temperature. Figure 9 shows the DHTT diagrams when holding time is 360 seconds, where the crystallization process of the above two mold fluxes has been completed. It was observed that the crystal layer of the Sample 1 is thicker than Sample 4; it indicated that using 10 pct BaO for the substitution of CaO to replace 10 pct B_2O_3 could inhibit crystallization. All the results are consistent with the TTT curves in Figure 4(e).

IV. CONCLUSIONS

Crystallization behavior of lime–alumina-based mold flux with C/A ratio of 2 was studied, and the effects of BaO substituting for CaO to replace B_2O_3 on the crystallization behavior were investigated as well. The specific conclusions are summarized as follows:

1. The results of CCT indicated that the crystallization property of mold flux was improved under the synergic effect of the combination of BaO and B_2O_3, and the mold flux Sample 4 with 10 pct BaO to replace B_2O_3 shows the weakest crystallization capacity.
2. The results of TTT indicated that single BaO would restrain crystallization dramatically especially in the low-temperature zone for Sample 4 due to the formation of $BaAl_2O_4$. The mold flux with mixture of BaO and B_2O_3 shows stronger crystallization capability especially in high-temperature zone due to the formation of CaF_2, while little effect on crystallization property in low-temperature zone. The results were consistent with CCT results. XRD analysis for above crystal phase was conducted for the explanation of above phenomena.
3. The DHTT images of Sample 1 and Sample 4 under the simulated thermal gradient for the same holding times were discussed. The results were in accordance with above conclusions, which added the reliability of this study.

ACKNOWLEDGMENTS

The financial support from NSFC (51274244, 51322405) and Hunan Excellent Young Scholar Funding (14JJ1005) is greatly acknowledged.

REFERENCES

1. B. Xie: Ph. D. Dissertation, Chongqing University, Chongqing, China, 2004.
2. K.C. Mills and A.B. Fox: *ISIJ Int*., 2003, vol. 43, p. 1479.
3. W. Wang, K. Blazek, and A. Cramb: *Metall. Mater. Trans. B*, 2008, vol. 39B, pp. 66–74.
4. Z. Zhang, G. Wen, and P. Tang: *ISIJ Int*., 2008, vol. 48 (6), pp. 739–46.
5. J. Liao, Y. Zhang, S. Sridhar, X. Wang, and Z. Zhang: *ISIJ Int*., 2012, vol. 52, p. 753.
6. H. Todoroki, T. Ishii, K. Mizuno, and A. Hongo: *Mater. Sci. Eng. A*, 2005, vols. 413–414, p. 121.
7. Y. Kanbe, T. Ishii, H. Todoroki, and K. Mizuno: *Int. J. Cast. Metal. Res*., 2009, vol. 22, p. 143.
8. H. Kim and I. Sohn: *ISIJ Int*., 2011, vol. 51, p. 1.
9. H.S. Park, H. Kim, and I. Sohn: *Metall. Mater. Trans. B*, 2011, vol. 42B, p. 324.
10. J. Cho, K. Blazek, M. Frazee, and H. Yin: *ISIJ Int*., 2013, vol. 53 (1), pp. 62–70.
11. K. Blazek, H. Yin, G. Skoczylas, M. McClymonds, and M. Frazee: *Iron Steel Technol*., 2011, vol. 8, pp. 231–40.
12. Q. Wang, D. Xie, and S. He: *Iron Steel Res. Int*., 2007, vol. 19 (6), pp. 38–41.
13. Y. Wang, F. Dong, and B. Wang: *Special Steel*, 2007, vol. 28 (2), pp. 22–23.
14. X. Yu: Ph. D. Dissertation, Chongqing University, Chongqing, China, 2011.
15. L. Zhou, W. Wang, D. Huang, J. Wei, and J. Li: *Metall. Mater. Trans. B*, 2012, vol. 43B, p. 925.
16. Y. Kashiwaya, C.E. Cicutti, and A.W. Cramb: Proc. Steelmaking Conf., Toronto, ON, Canada, Iron and Steel Society, 1998, pp. 185–91.
17. L. Zhou and W. Wang: *Metall. Mater. Trans. B*, 2012, vol. 43B, pp. 925–36.
18. S. Jung, G. Kim, and I. Sohn: *Trans. Indian. Inst. Met*., 2013, vol. 66 (5), pp. 577–85.
19. X. Yu: Ph D Dissertation, Chongqing University, Chongqing, China, 2011.